

Dependence of Magnetic Domain-Wall Motion on a Fast Changing Current

Lars Bocklage,^{1,*} Benjamin Krüger,^{2,†} Toru Matsuyama,¹ Markus Bolte,¹ Ulrich Merkt,¹
Daniela Pfannkuche,² and Guido Meier¹

¹*Institut für Angewandte Physik und Zentrum für Mikrostrukturforschung, Universität Hamburg,
Jungiusstrasse 11, 20355 Hamburg, Germany*

²*I. Institut für Theoretische Physik, Universität Hamburg, Jungiusstrasse 9, 20355 Hamburg, Germany*

(Received 26 June 2009; published 6 November 2009)

A dependence of current-induced domain-wall motion in nanowires on the temporal shape of current pulses is observed. The results show that the motion of the wall is amplified for alterations of the current on a time scale smaller than the intrinsic time scale of the domain wall which is a few nanoseconds in permalloy. This effect arises from an additional force on the wall by the spin-transfer torque due to a fast changing current and improves the efficiency of domain-wall motion. The observations provide an understanding for the efficient domain-wall motion with nanosecond current pulses.

DOI: 10.1103/PhysRevLett.103.197204

PACS numbers: 75.60.Ch, 72.25.Ba, 75.75.+a, 85.75.-d

Spin-polarized electrical currents exert a spin torque on the local magnetization of a ferromagnet [1]. The spin torque switches the magnetization in spin-valve nanopillars [2,3] or nanoislands [4] and moves domain walls beaded along a magnetic nanowire [5–7]. Domain walls play an important role in concepts towards high-density and ultrafast nonvolatile data-storage devices [8,9]. Efficient domain-wall motion is achieved for pulses in the nanosecond regime [10]. This is attributed to a stochastic behavior of pinning and depinning at material defects or at geometrical pinning sites [11,12] which determines the critical current density to move the domain wall. Therefore, an efficient depinning process is essential. Our results reveal the important contribution of the current's rise time to the motion and the depinning of domain walls and explain the observed efficient domain-wall motion for current pulses in the nanosecond regime.

In experiments, it was shown that a current with a special temporal shape can reduce the critical current density for domain-wall motion [11,13,14]. These experiments aim at resonant excitation of the wall. The resonant behavior depends on the pulse length, on a series of properly timed current pulses, or on a resonant alternating current that is applied to the wire. It was found theoretically that domain-wall motion driven by temporally varying spin-polarized currents depends not only on the current density but also on its time derivative [15,16]. This leads to the assumption that the rise time of a current pulse can have a similar effect on the critical density as a resonant excitation.

We perform experiments and analytical calculations on the influence of a temporally changing current density on the depinning probability is studied. An influence of the rise time can be found for fast rising current pulses. The time scale in which the rise time significantly affects the depinning probability is given by the damping time of the wall. The knowledge of the resonance frequency of the wall is

not necessary. This is especially important as the resonance frequency normally varies from pinning site to pinning site.

We investigate domain walls in a permalloy ($\text{Ni}_{80}\text{Fe}_{20}$) nanowire. The wire shown in Fig. 1(a) is 380 nm wide, 20 nm thick, and has a notch with a depth of about 120 nm. The notch is an artificial pinning site. The wire is contacted by gold leads indicated as L1 and L2. The curvature of the wire serves to reproducibly prepare a domain wall by applying a magnetic field of 100 mT at an angle of

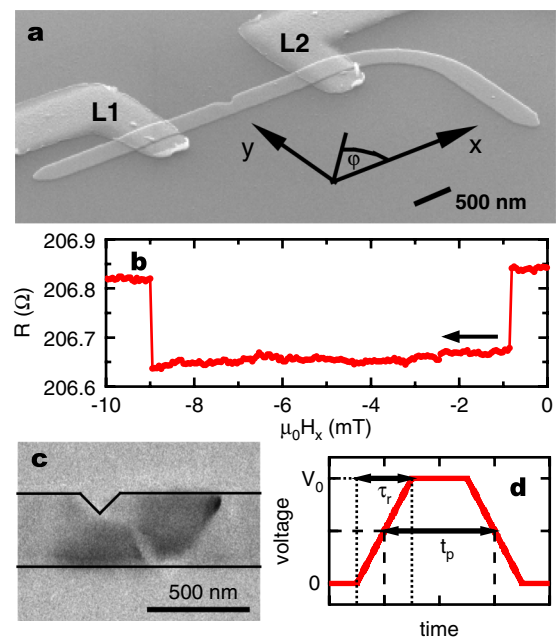


FIG. 1 (color online). (a) Scanning-electron micrograph of the permalloy wire. The gold contacts are indicated as L1 and L2. (b) Dependence of the resistance of the wire between contacts L1 and L2 on the magnetic field in x direction. The arrow indicates the sweep direction of the magnetic field. (c) Magnetic-force micrograph of a domain wall pinned at the notch. (d) Definition of the pulse length and rise time of the current pulse.

$\varphi = 80^\circ$ and switching the field off. Under the influence of an external magnetic field along the x direction (see Fig. 1) the domain wall moves to the notch and gets pinned at -0.81 mT, which is detected by the change of the anisotropic magnetoresistance. Measurements of the resistance between the gold contacts L1 and L2 show a sharp drop of about 0.2Ω as the domain wall enters the region between the gold contacts [see Fig. 1(b)] [17]. The sharp increase observed at -8.95 mT is given by the depinning of the domain wall from the notch due to the magnetic field. Magnetic-force microscopy confirms the pinning of the domain wall at the notch. In Fig. 1(c), a vortex wall is observed. The pinning and depinning fields are measured 10 times and are highly stable ($\sigma = 0.03$ mT) revealing that the same domain-wall type is repeatedly achieved. This is important as different domain-wall types have different depinning fields [18,19].

Figure 1(d) depicts the definition of the rise time and the pulse length. Within the rise time τ_r , the voltage increases to its maximal amplitude V_0 . The pulse length t_p is defined as the full width at half maximum. Therefore, the longest rise time achievable is equal to the pulse length, resulting in a triangular shape of the pulse. To measure the dependence of the depinning probability of the domain wall on the pulse shape, current pulses of different length and rise time are launched into the sample. First, a domain wall is prepared in the curvature by the field sequence described above and the resistance of the wire is measured. Then, a magnetic field along the x direction is applied in order to move the domain wall to the notch region followed by a second measurement of the resistance. Subsequently, a voltage pulse of $V_0 = -1$ V is launched into lead L2 resulting in a maximum current density of $|j| = 8.5 \times 10^{11}$ A/m² and the resistance is measured a third time. In this case, the electrons flow from contact L2 to L1 leading to a displacement of the wall in the same direction. From the difference in the resistances, the presence of a domain wall at the notch and its depinning due to the current pulse can unambiguously be determined. This sequence is measured 10 times for every set of parameters of magnetic field, pulse length, and rise time to determine the depinning probability.

Figure 2 shows the depinning probability of a head-to-head domain wall for pulse lengths of 5, 10, and 15 ns for different rise times and magnetic fields. For all three pulse lengths, the depinning probability shifts to higher fields as the rise time approaches the pulse length. The main difference between the three pulse lengths is a constant part in the depinning probability for long current pulses and short rise times where the probability does not change with changing rise time. This part is not observed for a pulse length of 5 ns. The same measurements can be performed for a tail-to-tail wall by inverting all magnetic fields in the sequence described above. Figure 3(a) shows the depinning probability for a tail-to-tail wall and a pulse length of 10 ns.

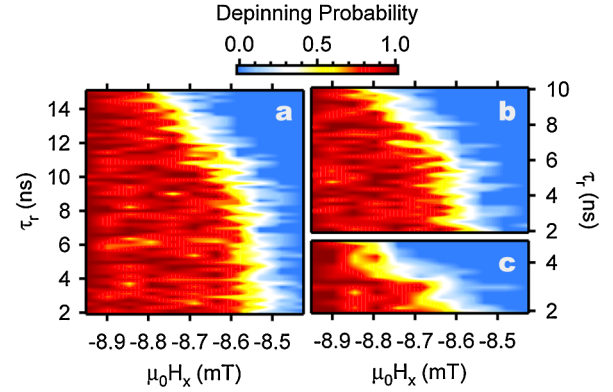


FIG. 2 (color online). Depinning probability of a head-to-head wall for different pulse lengths, rise times, and magnetic fields. The pulse lengths are (a) 15 ns, (b) 10 ns, and (c) 5 ns.

It shows the same behavior as the head-to-head domain wall depicted in Fig. 2(b).

Measurements of the depinning probability for constant rise time and changing pulse length are shown in Fig. 3(b). No dependence is observed on the pulse length. This is consistent with measurements of Thomas *et al.* [11] for the given direction of current and field. The measurement shows that a thermally induced depinning can be excluded for the observed dependence of the rise time. Pulses with constant length and varying rise time cause different Joule heating as the induced power is $P \propto V^2$ [see Figs. 3(c) and 3(d)], and calculations show that the amount of the deposited energy can change up to one third. However, the

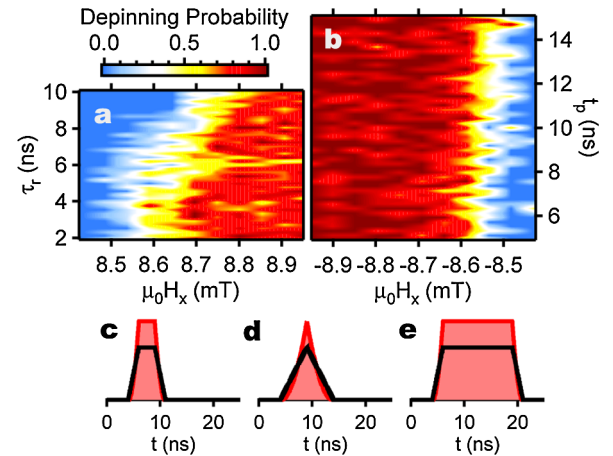


FIG. 3 (color online). (a) Depinning probability of a tail-to-tail wall for a pulse length of 10 ns for varying rise times and magnetic fields. (b) Depinning probability of a head-to-head wall for varying pulse lengths and magnetic fields at a constant rise time of 2 ns. (c)–(e) Scheme of the influence of the pulse profile on the induced energy. The black lines depict the current pulse. The areas represent the induced energy in the nanowire. The pulses have pulse lengths t_p and rise times τ_r of (c) $t_p = 5$ ns and $\tau_r = 2$ ns, (d) $t_p = 5$ ns and $\tau_r = 5$ ns, and (e) $t_p = 15$ ns and $\tau_r = 2$ ns.

change of the energy deposited due to a longer pulse is much more prominent than the change due to the rise time [see Figs. 3(c) and 3(e)]. Therefore, Joule heating can be excluded as the origin of the observed dependence of the depinning probability on the rise time. Thus, the observations are clearly attributed to the temporal change of the current.

For the analytical calculation, we approximate a transverse domain wall as a rigid particle. Then, a one-dimensional model, including the spin-torque terms of Zhang and Li [1], describes the motion of the domain wall. The wall is described by its position X and the out-of-plane tilting angle ϕ of the wall. The equations of motion for the domain wall are [15]

$$\dot{X} = -\frac{\lambda}{\alpha\tau_d}\phi + \frac{\lambda\gamma\alpha}{1+\alpha^2}H(X) - \frac{1+\alpha\xi}{1+\alpha^2}b_j j \quad (1)$$

and

$$\dot{\phi} = -\frac{\gamma}{1+\alpha^2}H(X) - \frac{\phi}{\tau_d} + \frac{\xi-\alpha}{\lambda(1+\alpha^2)}b_j j. \quad (2)$$

Here, γ is the gyromagnetic ratio, α is the Gilbert damping parameter, ξ is the nonadiabaticity, b_j is the coupling constant between the current and the magnetization, λ is the domain-wall width, and $H(X)$ is the magnetic field in the wire direction that varies slowly on the length scale of the domain wall. The damping time $\tau_d = \frac{\mu_0 M_s (1+\alpha^2)}{2\gamma\alpha K_\perp}$ depends on the saturation magnetization M_s and on the perpendicular anisotropy K_\perp of the wire. During the damping time, the free wall slows down to e^{-1} of its initial velocity. The magnetic field $H = H_{\text{ext}} + H_{\text{pin}}$ consists of the external field and the pinning field [20]. The pinning field $H_{\text{pin}} = -\frac{\alpha\tau_d}{\lambda\gamma m'} \frac{dE}{dX}$ is expressed by the pinning potential E and by the domain-wall mass $m' = \frac{2\alpha S\mu_0 M_s \tau_d}{\lambda\gamma}$ with the cross section S of the wire. The sign of the magnetic field differs from that given in Ref. [15] because we are looking at a head-to-head wall instead of a tail-to-tail wall. Equations (1) and (2) can be decoupled [21] resulting in

$$\begin{aligned} \frac{F}{m'} = \ddot{X} = & -\frac{\dot{X}}{\tau_d} - \frac{1}{m'} \frac{dE}{dX} + \frac{\lambda\gamma}{\alpha\tau_d} H_{\text{ext}} \\ & + \frac{\lambda\gamma\alpha}{1+\alpha^2} \dot{H}_{\text{ext}} - \frac{\xi b_j}{\alpha\tau_d} j - \frac{1+\alpha\xi}{1+\alpha^2} b_j j. \end{aligned} \quad (3)$$

The contributions of current-induced motion are the last two terms (spin-torque terms). The force F on the wall does not only depend on the current density but also on its time derivative, in major difference to the classical analogue, e.g., in hydrodynamics. The rise-time dependence of current-induced depinning follows from the time dependent spin-torque term in Eq. (3). For a nonadiabaticity parameter ξ that is equal to the Gilbert damping α [12,22], the spin-torque terms reduce to $\dot{X}_{\text{sp}} = -\frac{b_j}{\tau_d} j - b_j j$. Both forces are in the same order of magnitude for a

fast changing current on the time scale of the damping time. Figure 4 shows the contributions of both the constant part of the current and its time derivative. The contribution of the time derivative is significant. The force caused by the magnetic field also depends on the time derivative of the field; however, the ratio is only about 10^{-4} . In the present geometry, Oersted fields are negligible [23]. Equation (3) is valid for a transverse wall. Our micromagnetic simulations show that a vortex wall can also be described by this linear equation of motion using effective parameters.

Figures 5(a) and 5(b) show the simulated displacements of tail-to-tail transverse and vortex walls versus time due to a pulse with the rise time $\tau_r = 0$ and $\alpha = \xi = 0.01$. The simulations of the transverse wall are performed in a wire with 10 nm thickness and 120 nm width. The cross section is 20 nm \times 120 nm for the vortex walls [24]. The material parameters of permalloy, i.e., saturation magnetization $M_s = 8 \times 10^5$ A/m, exchange constant $A = 1.3 \times 10^{-11}$ J/m, and gyromagnetic ratio $\gamma = 2.211 \times 10^5$ m/C are used. In the simulation, the spin-polarized current density Pj and the magnetic field H are -4×10^{11} A/m² and -50 A/m for the transverse wall and -4×10^{11} A/m² and -500 A/m for the vortex walls, respectively. The simulated data are fitted with the analytical model resulting in a damping time of 0.8 ns for the transverse wall and of 8.2 and 8.1 ns for the right- ($cp = 1$) and left-handed ($cp = -1$) vortex wall, respectively. The different initial velocities of the two vortex walls with different handedness are due to the different deflections of the vortex core by the magnetic field [25,26]. All three wall types are described by the analytical model. For all three wall types, the reaction of the wall on current is much faster than the reaction on magnetic field. The pinning

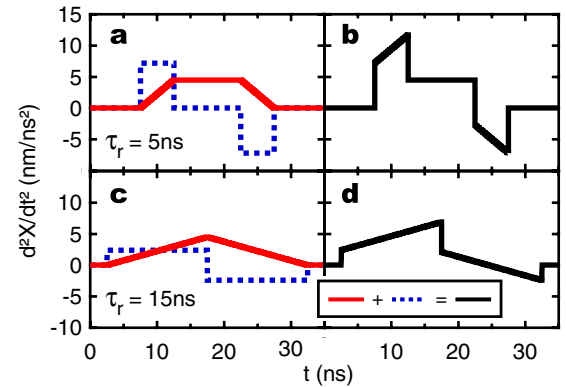


FIG. 4 (color online). Acceleration of a domain wall with a damping time of 8 ns due to a current pulse of -1×10^{12} A/m² and a width of 15 ns. A coupling constant b_j of 3.6 $\times 10^{-11}$ m³/C with a spin polarization P of 0.5 is assumed. The rise time of the pulse is 5 ns in (a) and (b) and 15 ns in (c) and (d). (a) and (c) Acceleration of the domain wall due to the constant part (solid red line) and the time derivative (dotted blue line) of the current. (b) and (d) Resultant acceleration due to the current.

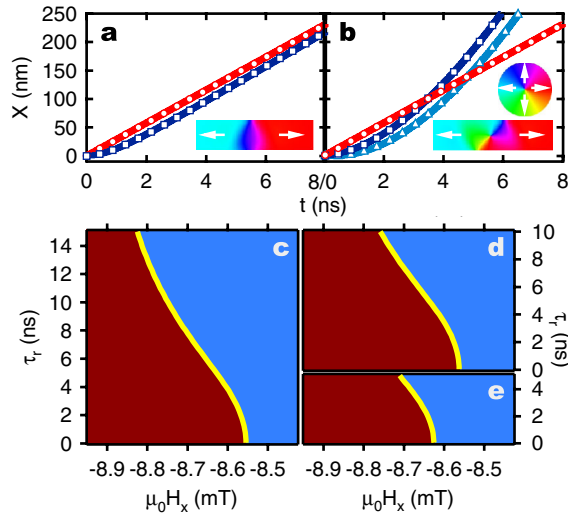


FIG. 5 (color online). Simulated current-induced (dots), simulated field-induced (squares, triangles), and corresponding analytically calculated (lines) displacements (a) for a transverse wall and (b) for left-handed (squares) and right-handed (triangles) vortex walls. The inset shows the simulated magnetization of the walls. (c)–(e) Calculated boundary for the depinning of a vortex wall for different pulse lengths, rise times, and magnetic fields. The pulse lengths are (c) 15 ns, (d) 10 ns, and (e) 5 ns.

force on the domain wall is mediated by the pinning field. If the rise time is small compared to the damping time ($\tau_r \ll \tau_d$), the reaction of the domain wall on the pinning field is much slower than the reaction on the varying current density. As a consequence, the domain wall can leave the pinning potential before the pinning field can stop the motion of the wall, leading to a reduction of the external field necessary for depinning.

Figures 5(c)–5(e) show the boundary for depinning of the vortex wall calculated from the analytical model [27]. With an appropriate pinning potential [21], the experimental data shown in Fig. 2 are well reproduced. Slight deviations between the experiment and the analytical model can be attributed to the modeled pinning potential and to the internal magnetic structure of the vortex wall which can change due to a current pulse [6,12,18]. Both can affect the actual depinning behavior at the notch.

The model explains why domain walls move only temporally close to the rise time [10]. It also explains the low averaged domain-wall velocities for long current pulses. The pulse exerts an additional force on the domain wall during the rise time which assists the depinning. If the constant part of the current is not capable of preventing pinning, the moving wall stops depending on the pinning potential and on the current density. Then, another pulse is necessary to depin the wall.

In summary, we have observed experimentally and described theoretically that a current has two contributions to

domain-wall motion. One part arises from the absolute value of the current. The other part is proportional to the temporal change of the current. The results show that rise times smaller than the damping time of the wall lead to an efficient depinning process. The findings should be independent of the origin of pinning at material defects or artificial pinning sites, generally apply to current-induced domain-wall motion, and are important for possible memory devices.

We would like to thank Michael Martens and Judith Moser for magnetic-force microscopy. Financial support of the Deutsche Forschungsgemeinschaft via the Sonderforschungsbereich 668 and via the Graduiertenkolleg 1286 as well as the city of Hamburg via the Cluster of Excellence Nano-Spintronics is gratefully acknowledged.

*lbocklag@physnet.uni-hamburg.de

†bkrueger@physnet.uni-hamburg.de

- [1] S. Zhang and Z. Li, Phys. Rev. Lett. **93**, 127204 (2004).
- [2] E. B. Myers *et al.*, Science **285**, 867 (1999).
- [3] J.P. Strachan *et al.*, Phys. Rev. Lett. **100**, 247201 (2008).
- [4] S. Krause *et al.*, Science **317**, 1537 (2007).
- [5] A. Yamaguchi *et al.*, Phys. Rev. Lett. **92**, 077205 (2004).
- [6] M. Kläui *et al.*, Phys. Rev. Lett. **95**, 026601 (2005).
- [7] M. Hayashi *et al.*, Science **320**, 209 (2008).
- [8] D.A. Allwood *et al.*, Science **309**, 1688 (2005).
- [9] S.S.P. Parkin *et al.*, Science **320**, 190 (2008).
- [10] S. Yang and J.L. Erskine, Phys. Rev. B **75**, 220403(R) (2007).
- [11] L. Thomas *et al.*, Nature (London) **443**, 197 (2006).
- [12] G. Meier *et al.*, Phys. Rev. Lett. **98**, 187202 (2007).
- [13] L. Thomas *et al.*, Science **315**, 1553 (2007).
- [14] D. Bedau *et al.*, Phys. Rev. Lett. **99**, 146601 (2007).
- [15] B. Krüger *et al.*, Phys. Rev. B **75**, 054421 (2007).
- [16] T. Suzuki *et al.*, J. Appl. Phys. **103**, 113913 (2008).
- [17] M. Bolte *et al.*, Phys. Rev. B **72**, 224436 (2005).
- [18] M. Hayashi *et al.*, Phys. Rev. Lett. **97**, 207205 (2006).
- [19] M.-Y. Im *et al.*, Phys. Rev. Lett. **102**, 147204 (2009).
- [20] L. Bocklage *et al.*, Phys. Rev. B **78**, 180405(R) (2008).
- [21] See EPAPS Document No. E-PRLTAO-103-014944 for supplementary information about the sample preparation, the experimental setup, and the analytical model. For more information on EPAPS, see <http://www.aip.org/pubservs/epaps.html>.
- [22] M. Hayashi *et al.*, Phys. Rev. Lett. **96**, 197207 (2006).
- [23] M. Bolte *et al.*, Phys. Rev. Lett. **100**, 176601 (2008).
- [24] Y. Nakatani *et al.*, J. Magn. Magn. Mater. **290**, 750 (2005).
- [25] B. Krüger *et al.*, Phys. Rev. B **76**, 224426 (2007).
- [26] S. Bohlens *et al.*, Appl. Phys. Lett. **93**, 142508 (2008).
- [27] Equation (3) written with effective parameters is $\dot{X} = -\frac{X}{\tau_d} + \frac{C_1}{\tau_d}H + C_2\dot{H} + \frac{C_3}{\tau_d}j + C_4\dot{j}$. The parameters for the vortex wall used in the calculation are $\tau_d = 8$ ns, $C_1 = 0.28$ m²/C, and $C_3 = C_4 = -b_j = -3.62 \times 10^{-11}$ m³/C.